

Evaluating resampled and fused Sentinel-2 data and machine-learning algorithms for mangrove mapping in the northern coast of Qeshm island, Iran

Ali Reza Soffianian¹, Neda Bihamta Toosi¹, Ali Asgarian¹,
Hervé Regnaud², Sima Fakheran¹, Lars T. Waser³

1 Department of Natural Resources, Isfahan University of Technology, Isfahan, 84156-83111, Iran **2** LETG – Littoral, Environnement, Télédétection, Géomatique UMR 6554, Rennes, France **3** Swiss Federal Institute for Forest, Snow and Landscape Research WSL, 8903 Birmensdorf, Switzerland

Corresponding author: Neda Bihamta Toosi (n.bihamtaitoosi@na.iut.ac.ir, nbihamta2010@gmail.com)

Academic editor: Javier Martínez-López | Received 11 July 2022 | Accepted 17 November 2022 | Published 20 March 2023

<https://zoobank.org/DAA2A509-8970-4D50-BE2D-5283578AE395>

Citation: Soffianian AR, Toosi NB, Asgarian A, Regnaud H, Fakheran S, Waser LT (2023) Evaluating resampled and fused Sentinel-2 data and machine-learning algorithms for mangrove mapping in the northern coast of Qeshm island, Iran. *Nature Conservation* 52: 1–22. <https://doi.org/10.3897/natureconservation.52.89639>

Abstract

Mangrove forests, as an essential component of the coastal zones in tropical and subtropical areas, provide a wide range of goods and ecosystem services that play a vital role in ecology. Mangroves are globally threatened, disappearing, and degraded. Consequently, knowledge on mangroves distribution and change is important for effective conservation and making protection policies. Developing remote sensing data and classification methods have proven to be suitable tools for mapping mangrove forests over a regional scale. Here, we scrutinized and compared the performance of pixel-based and object-based methods under Support Vector Machine (SVM) and Random Forest (RF) algorithms in mapping a mangrove ecosystem into four main classes (Mangrove tree, mudflat, water, and sand spit) using resampled and fused Sentinel-2 images. Additionally, landscape metrics were used to identify the differences between spatial patterns obtained from different classification methods. Results showed that pixel-based classifications were influenced heavily by the effect of salt and pepper noise, whereas in object-based classifications, boundaries of land use land cover (LULC) polygons were smoother and visually more appealing. Object-based classifications, with an excellent level of kappa, distinguished mudflat and sand spit from each other and from mangrove better than the pixel-based classifications which obtained a fair-to-good level of kappa. RF and SVM performed differently under comparable circumstances. The results of landscape metrics comparison presented that the classification methods can be affected on quantifying area and size metrics. Although the results supported the idea that fused Sentinel images may provide better results in mangrove LULC

classification, further research needs to develop and evaluate various image fusion approaches to make use of all Sentinel's fine resolution images. Our results on the mapping of mangrove ecosystems can contribute to the improvement of management and conservation strategies for these ecosystems being impacted by human activities.

Keywords

image fusion, landscape metric, mangroves, object-based classification, Sentinel-2

Introduction

Mangroves offer a considerable array of ecosystem goods and services including habitat and nursery for plant and animal, biodiversity, water quality maintenance, storm buffering, flood and flow control, fisheries, recreation, tourism, and so forth (Kuenzer et al. 2011; Salem and Mercer 2012; Savari et al. 2022). With an area of about 140,000 km², they account for less than 1% of all tropical forests and less than 0.4% of the total global forest estate (Giri et al. 2011). Conservation and management of mangrove ecosystems ties significantly with quantifying and valuing their ecosystem services using a wide variety of information, especially remotely sensed-derived land use land cover (LULC) data (Grêt-Regamey et al. 2015). One of the most frequently raised questions in this research area is to find out which combinations of image(s) and processing technique(s) can likely elicit the desired results for a specific issue (Ho et al. 2016; Olmanson et al. 2016; Sanli et al. 2017), especially for LULC classification, as one of the most primary and important applications of remote sensing (Lillesand et al. 2014). The majority of studies dealing with this concern focused their attention on certain landscapes such as impervious urbanized areas (Li et al. 2014; Poursanidis et al. 2015), while this agenda has not been well addressed yet in other highly dynamic and heterogeneous landscapes such as mangrove ecosystems, facing researchers with the challenge of selecting the apt imagery data and classification techniques in their research. A range of low- to high-resolution aerial images (Brown et al. 2018), hyperspectral images (Kuenzer et al. 2011), Synthetic Aperture Radar (SAR) data (Zhang et al. 2018), and Light Detection and Ranging (LiDAR) data (Olagoke et al. 2016) have been used to map the extent and distribution of mangrove cover classes. In the past decade, data have become available from Very High-Resolution (VHR) satellites, such as Worldview-2 and Pléiades-1, leading to improved mapping of mangrove cover classes (Proisy et al. 2018). However, the main limiting factor is the high cost of data acquisition.

As our literature review on English articles published since 2011 (Fig. 1) indicates, most studies on LULC classification of mangrove ecosystems narrowed their image selection down to Landsat mainly because it offers free and open access to its data archive (Toosi et al. 2019). Such a policy recently applied to some space missions, especially the new Sentinel program by the European Space Agency (ESA) (Wulder et al. 2012), enabled scholars to access a broader range, and even better, free image resources. The Multi-spectral Instrument (MSI) onboard Sentinel-2 is

equipped with the same push-broom instrument as Landsat 8 but has a higher spatial, temporal and spectral resolution (Sothe et al. 2017). In addition to the type of sensor, the selection of the right classification method is another challenging task influencing the classification outcomes. These methods are broadly categorized into pixel-based and object-based methods which are envisaged to perform differently under similar circumstances (Hussain et al. 2013). In pixel-based methods, each pixel is considered as the numerical basis for image classification, while object-based methods rely on a number of contiguous pixels with homogeneous spectral and spatial attributes as the basic classification element (known as objects or segments) to perform a categorization task (Blaschke et al. 2008; Blaschke 2010). Object-based methods were found to be more effective in classifying high spatial resolution images such as IKONOS, GeoEye, QuickBird, and SPOT 6/7, however, recent literature showed their promising utility for classifying medium resolution images such as Landsat and Sentinel (Blaschke et al. 2008). Fig. 1 displays the classification methods for the mapping of mangrove ecosystems. In this Figure, we divided the classification methods into main types: (1) classification technique, (2) classification algorithms. As given in fig. 1, the majority of studies on mangrove LULC classification relied on pixel-based methods and a very limited, but increasingly growing, attention has been given to object-based methods (Wang et al. 2004; Vo et al. 2013).

Furthermore, the algorithm by which a classifier is developed is also another key factor affecting the classification results. These algorithms are divided into parametric and nonparametric groups. Nonparametric methods allow training data to more robustly participate in the process of image classification and have a higher potency than nonparametric ones (Mountrakis et al. 2011; Ranaie et al. 2018). According to the literature review (Fig. 1), Maximum Likelihood (ML) from the

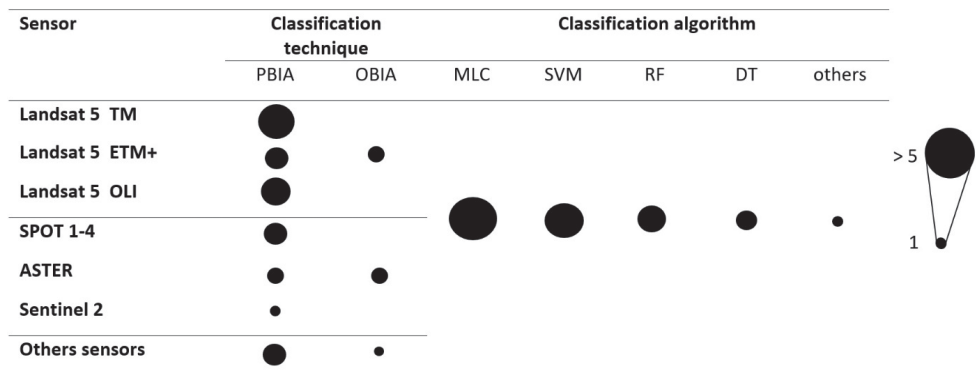


Figure 1. PBIA: Pixel-based image analysis; OBIA: Object-based image analysis; MLC: Maximum likelihood classification; SVM: Support Vector Machine; RF: Random forest; DT: Decision Tree; X: Number of articles.

Figure 1. PBIA: Pixel-based image analysis; OBIA: Object-based image analysis; MLC: Maximum likelihood classification; SVM: Support Vector Machine; RF: Random Forest; DT: Decision Tree; X: Number of articles.

group of parametric algorithms and Support Vector Machine (SVM) and RF from the group of nonparametric algorithms have been more interested in mapping mangrove ecosystems. Recently, neural networks and deep learning as machine learning algorithms have been developed in the research field (Pham et al. 2019a). Landscape metrics are powerful tools for quantifying spatial patterns that can help better understand the relationships between patterns and ecosystem processes. According to many studies, landscape metrics have various applications which can be categorized into the following six groups: a) biodiversity and habitat assessment, b) Water quality estimation, c) analysis of spatial pattern and its changes d) evaluation of urban landscape pattern and road network e) aesthetics of landscape f) management (Bozorgi et al. 2020). They are also useful for sustainable landscape planning and monitoring (Bihamta Toosi et al. 2012). Thematic maps resulting from image processing are commonly used to evaluate spatial patterns (Forman and Godron 1986).

Differences in spatial patterns identified in thematic maps affect the results of land use metrics (Uuemaa et al. 2013). This study aims to add to the small but growing body of research currently available in this area by comparing the performance of a combination of methods, algorithms, and imagery data in classifying mangrove ecosystems of Qeshm Island in the Persian Gulf, Iran. Additionally, to identify the differences between spatial patterns that were obtained from pixel-based and object-oriented classification methods, we used landscape metrics at different levels for the classification maps with the highest overall accuracy.

Material and methods

Study area

The study area of this research encompasses part of mangrove ecosystems located in the northwest of Qeshm Island in the Persian Gulf, Iran. This island is situated 20 km from the Bandar-Abbas Port in the Strait of Hormuz (Hormozgan Province) and spans over 26°40'N–27°00'N longitude and 55°20'E–55°50'E latitude. With an area of approximately 1490 km², Qeshm is the largest island in the Persian Gulf (2.5 times larger than the second biggest Island: Bahrain Country). About 90% of Iranian mangrove forests are located in the margins of the island's northwestern estuaries (Zahed et al. 2010). In addition to patchy mangrove trees, muddy areas which are formed by the deposition of alluvium along the estuaries (mudflat), groundwater seepage-impacted bare soils (sand spit) and shallow waters are another important land cover type found in these mangrove ecosystems. Mangrove ecosystems of the region are designated as a biosphere reservoir (Hara Protected Area) by UNESCO's Man and Biosphere Program (MAB) and as an international wetland according to Ramsar Convention (Zarezadeh et al. 2017; Bihamta Toosi et al. 2020). Fig. 2 shows the layout of the study area.

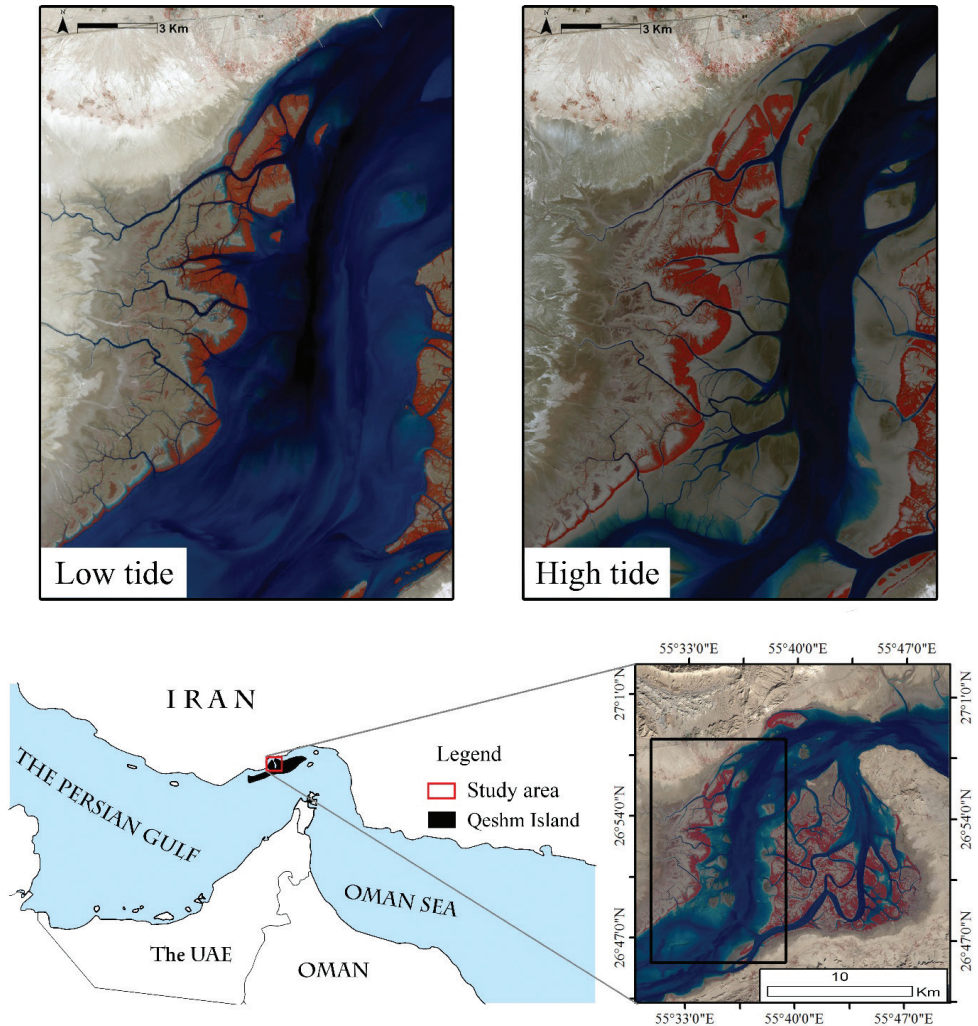


Figure 2. Location of the study area.

Data

The workflow of this study is designed to utilize two Sentinel-2 MIS images (table 1). The onboard MSI consists of 13 spectral bands with four bands at 10 m, six bands at 20 m and three bands at 60 m spatial resolution (Wang et al. 2016).

One Sentinel-2 MIS image acquired at the time of the highest tidal level (December 10, 2017) was used to produce a radiometric mask distinguishing the study area from the surrounding bare lands and the other one obtained at the time of the lowest tidal level (November 15, 2017) was used for mangrove LULC classification. In this study 10 m and 20 m resolution bands were utilized for classification.

In addition to imagery data, a total of 170 GPS reference points (Garmin 629sc) were obtained close to the image acquisition time to evaluate the classification accuracy during the field survey. In doing so, a special attention was given to the positional error which was frequently regarded as one of the main sources of uncertainty in assessing the classification accuracy (Lunetta and Lyon 2004; Congalton and Green 2008). Additionally, some points were selected from Spot 6/7 and Worldview-2 data based on visual image analysis to raise the number of reference points for different types of LULC.

Table 1. List the characteristics of 3 spatial resolution of the MSI.

Spatial Resolution (m)	Band Number	S2A		S2B	
		Central Wavelength (nm)	Bandwidth (nm)	Central Wavelength (nm)	Bandwidth (nm)
10	2	496.6	98	492.1	98
	3	560.0	45	559	46
	4	664.5	38	665	39
	8	835.1	145	833	133
20	5	703.9	19	703.8	20
	6	740.2	18	739.1	18
	7	782.5	28	779.7	28
	8a	864.8	33	864	32
	11	1613.7	143	1610.4	141
60	12	2202.4	242	2185.7	238
	1	443.9	27	442.3	45
	9	945.0	26	943.2	27
	10	1373.5	75	1376.9	76

Methods

Image preprocessing

To enhance the quality of images and perform more accurate image classifications, atmospheric and radiometric correction was conducted by the Fast Line-of-sight Atmospheric Analysis of Hypercubes (FLAASH) module in ENVI 5.4. This module relies on MODTRAN (Moderate resolution atmospheric Transmission) which is a radiative atmospheric propagation model for the spectral range of 200–100,000 nm (Ballestrin and Marzo 2012). A radiometric mask was then produced using the Normalized Difference Water Index (NDWI) to distinguish the mangrove ecosystem areas from the surrounding bare soils. This index was proposed by McFeeters (1996) and has been successfully applied in detecting changes in water bodies by integrating the reflectance of objects in the green (ρ_{green}) and near infrared (ρ_{NIR}) spectrum (Eq. 1). This index is also sensitive to the water content of vegetation canopies (Xu 2006). Given the reflective behavior of water in the infrared spectrum, NDWI obtains negative values in dry unvegetated bare soils (minimum of -1) and increases with the rise in the amount of

water and vegetation intensity (maximum of +1) (Xu 2006). In order to define the classification extent, all of the four main LULCs constituting the mangrove ecosystems (mangrove tree, mudflat, sand spit, and water) were well discriminated from the surrounding bare soils by assigning a threshold NDWI value of 0.00.

$$NDWI = \frac{\rho_{green} - \rho_{NIR}}{\rho_{green} + \rho_{NIR}} \quad (1)$$

Image fusion and resampling

This task enhances the quality and interpretation capability of the images and, in turn, may produce more accurate classification results (Jiang et al. 2013; Qadri et al. 2017). A variety of data fusion techniques have been developed to date which can be broadly classified as Component Substitution (CS) and Multi-Resolution Analysis (MRA) methods (Wang et al. 2016). These methods (known as PAN-sharpening methods) rely on a single FW image and are more applicable for fusion of, for example, Landsat which collects a single FW band (known as the panchromatic). Sentinel-2, however, obtains four fine pixel size bands and requires a different fusion approach to PAN-sharpening techniques.

In this study, the method of Gašparović and Jogun (2018) was employed for this purpose. In doing so, the 60 m resolution bands were first excluded from the analysis. 20 m bands were then placed into two groups in terms of spectral range. Band 8a, 11, and 12 fell into one group and band 5, 6, and 7 into another. Band 8 and the linear combination of band 4 and 8 were considered as the FW band for the first and second group, respectively (for a more detailed description of the intuition behind this method, readers are referred to Gašparović and Jogun (2018)). The Intensity-Hue-Saturation (HIS) method was then used to perform data fusion. According to this method, CN bands were first transformed from RGB (Red-Green-Blue) to HIS color space. The hue and saturation bands were then resampled to FW band and, ultimately, the resulting bands were re-transformed to the RGB space (Choi et al. 2006). In addition to fusion, image resampling was also carried out on the original bands using the nearest neighbor method and the second-order polynomial transformation to downscale 20 m resolution bands to 10 m using 28 control points which achieved an acceptable RMSE value of 0.2. Hereafter, these two sets were referred to as the fused and resampled images.

Spectral indices

NDWI (see section 2.3.1), Normalized Difference Vegetation Index (NDVI), and Normalized Difference Built-up Index (NDBI) were produced to support the image bands through mangrove LULC classification. Several studies used the NDVI to improve monitoring of the mangroves (Pham et al. 2019b). A sufficient number of studies suggest that a combination of image bands with spectral indices can improve the accuracy of image classification, especially in object-based classifications (Tong Yang et al. 2015). The results of studies have shown that the use of NDVI for discriminating

mangrove species using different remote sensing data is affected by spatial resolution. The higher spatial resolutions produce higher accuracy (Lee and Yeh 2009; Pham et al. 2019b). This index is computed using Eq. 2 where (ρ_{red}) and (ρ_{NIR}) are the spectral reflectance acquired in the red and near-infrared spectrum, respectively. NDBI has been used frequently for identifying bare and semi-bare soils and built-up lands in various studies (As-Syakur et al. 2012; Bihanta et al. 2019) by substituting the spectral reflectance of objects in short wave infrared (ρ_{SWIR}) and near infrared spectrum in Eq. 3.

$$NDVI = \frac{\rho_{NIR} - \rho_{Red}}{\rho_{NIR} + \rho_{Red}} \quad (2)$$

$$NDBI = \frac{\rho_{SWIR} - \rho_{NIR}}{\rho_{SWIR} + \rho_{NIR}} \quad (3)$$

Image segmentation

Image segmentation splits the image into small polygons in alignment with the objects of interest in the study area (Blaschke et al. 2008). It performs by defining three tuning parameters: shape, compactness, and scale (Srivastava et al. 2015). Image segmentation was carried out using the Multiresolution Segmentation Algorithm (MRS) embedded in the eCognition software. MRS is the most popular and important algorithm for this purpose (Drăguț et al. 2014) which basically relies on a key controlling factor known as Scale Parameter, allowing users to select the best-performing values for the above-mentioned three parameters (shape, compactness, and scale) by trial-and-error (Benz et al. 2004; Drăguț et al. 2014).

Image classification

A number of 356 polygons were sampled through visual interpretation of the color composites of the Sentinel images and a Spot image scene acquired on December 20, 2016. In doing so, a special attention was also given to the mean reflectance of each segment whereby those which most correspond to the pre-defined spectral signature of the respective LULC class were chosen as sample polygons. Sample polygons of each LULC class were randomly split into two groups, each containing 78 samples for mangrove tree, 54 for mudflat, 25 for sand spit, and 21 for water. One group which was used to train the algorithms was evaluated in terms of the divergence between the classes and the other group was used for accuracy assessment. Given the promising results of non-parametric algorithms (see the introduction section), RF and SVM as the two well-known and commonly used classifiers in this case (Mountrakis et al. 2011; Belgiu and Drăguț 2016) were employed for mangrove LULC classification. These algorithms are briefly described in the following paragraphs. The classification results were finally evaluated and compared by calculating accuracy indices including kappa coefficient, overall accuracy, and user's and producer's accuracies (see Congalton and Green (2008)) from confusion matrices. Fig. 3 shows the steps undertaken in this research.

Support Vector Machine (SVM)

SVM was pioneered by Fisher in 1936 to reduce the error rate of discriminating training data based on the Statistical Learning Theory and then expanded by Cortes and Vapnik (1995) as a classification algorithm. This algorithm has broad applications in regression analysis, classification, and clustering. The basic principle of SVM is to draw an optimal separating linear line in which the distance between the marginal distribution of features from each class and the hyperplane is maximized (Cristianini and Shawe-Taylor 2000; Wang 2005). In image classification, SVM distributes each training sample as a point in an n-dimensional space where each dimension corresponds to an image band and uses an optimization algorithm to find surfaces (known as hyperplane) which best distinguish between the points with the same LULC labels (Mountrakis et al. 2011). One of the most remarkable characteristics of this algorithm is that it concurrently maximizes the geometric margin and minimizes the experimental classification error and thus is known as Maximal Margin classifier (Cristianini and Shawe-Taylor 2000).

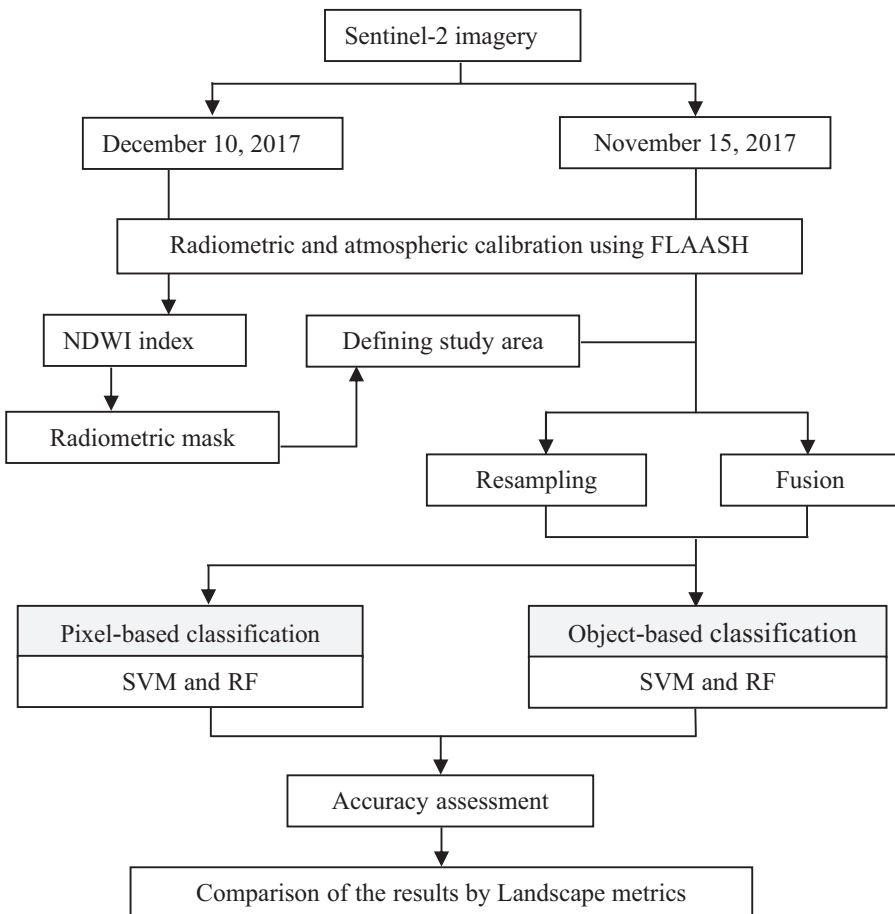


Figure 3. Research approach as a flowchart.

Random Forest (RF)

RF (also known as random decision forests) was first introduced by Breiman (2001) to solve the problems of classification. This algorithm consists of a collection of decision trees (a forest). Trees in this algorithm are built using a random subset of training data through bootstrap sampling with replacement (known as bagging). The trees are then grown independently and those having a high variance and low bias are chosen as the best performing trees while the others are pruned (Breiman 2001; Belgiu and Drăguț 2016). Through this process, each tree casts a vote to attribute the most frequent class to an input vector and the votes of all trees are finally combined, counted and the class containing the majority of votes are labeled as a new classification (Angadi et al. 2013).

Two-thirds of training data are used for generating trees (known as in bag samples) and the remaining one-third for cross-validation which evaluates the performance of the RF model (Belgiu and Drăguț 2016).

Comparison of spatial pattern analysis

A review of the literature shows that the metrics most commonly used to study forest ecosystems include metrics of area, shape, proximity, and diversity (Tran and Fischer 2017). In this study, four metrics of number of patches (NP), Patch Density (PD), Large Shape Index (LSI) and Mean Patch Area (AREA-MN) were selected for comparison. At the class level, the metrics Percentage of Landscape (PLAND), Number of patches (NP), Area-Weighted Mean Fractal Dimension Index (FRAC-AM) and Mean Euclidean Nearest Neighbor Distance (ENN-MN) were selected. Seven metrics including Total Area (TA), Edge Density (ED), Mean Patch Area (AREA-MN), Number of patches (NP), Patch Density (PD), Contagion (CONTAG) and Shannon's Diversity Index (SHDI) were selected at the landscape level. Table 2 shows the selected landscape metrics calculated using Fragstats 4.2 software.

Results

The accuracy of object-based classification depends significantly on the quality of image segmentation. In this research, segments were generated through frequent trial-and-error and visual interpretation of the outputs. Accordingly, the scale factor was assigned to a value of 5. The influence weight of NDVI was considered twice greater than other bands (2:1). The shape and compactness factors were also kept constant as 0.1. The resampled and fused Sentinel-2 images were then classified using pixel- and object-oriented RF and SVM algorithms. Table 3 shows the area of LULC classes. According to these results, the total area specified to each class varied significantly among the classifications. The least difference between the areas devoted to each LULC class was observed for water class with the maximum area difference of 1007 ha (3.6% difference) and the biggest one with the maximum area difference of approximately 3,150 ha (20.2% difference) was obtained for sand spit class. One of the most intriguing results

Table 2. Descriptions of landscape metrics used in the study (Mc Garigal and Marks 1995).

Category	Name	Acronym/Units	Description
Area	Mean Patch Area	AREA-MN/ Meter	Description Average area of all patches in the SU (ha)
	Percentage of Landscape	PLAND/ Percent	PLAND made up of the corresponding class
	Total Area	TA/ Hectares	TA includes any internal background present.
	Edge Density	ED/ Meters per hectare	ED equals the sum of the lengths (m) of all edge segments involving the corresponding patch type.
Shape	Area Weighted Mean Patch Fractal Dimension	FRAC-AM/ None	FRAC reflects shape complexity across a range of spatial scales
	Patch density	PD/ Number per 100 hectares	PD of a certain class divided by the total landscape area n patches per ha
Subdivision	Number of patches	NP/ None	NP of the corresponding patch type (class).
	Euclidean nearest neighbor distance	ENN-MN/ Meters	MNN increases when the mean distance of patches from each type is increased.
Aggregation	Landscape shape Index	LSI/ None	A perimeter-to-area ratio that measures the overall geometric complexity of the landscape (landscape level)
	Contagion	CONTAG/ Percent	Higher CONTAG values represents a landscape with less dispersed and more contiguous units.
Diversity	Shannon's Diversity Index	SHID/ None	SHDI increases with the increase in evenness and richness of patch types.

Table 3. The area of LULC classes.

Algorithm	LULC class	Area (ha)			
		Pixel-based classification		Object-based classification	
		Resampled image	Fused image	Resampled image	Fused image
RF	Wet area	15536.4	15099.2	13184.5	13612.6
	Mangrove	9249.8	9032.1	8804.4	8543.8
	Mudflat	13974.4	15184.0	16845.1	16957.2
	Water	26906.4	26351.6	26832.8	26553.2
SVM	Wet area	12389.3	14073.7	12872.8	13184.5
	Mangrove	8979.6	9293.2	8846.1	8804.4
	Mudflat	17039.3	15549.7	16935.7	16845.1
	Water	27258.7	26750.3	27012.1	26832.8

derived from table 2 is the difference between object-based and pixel-based classifications in exploring mangrove trees, according to which the area (the number of pixels) specified to this class through pixel-based classifications was relatively larger than that of delineated under object-based classifications. The spatial difference between object-based and pixel-based classifications is shown in a close-up of the central part of the study area in fig. 4, which illustrates parts of all four LULC classes (mangrove, water, sand spit, and mudflat). As seen from fig. 4, a glaring difference was found between the spatial pattern of LULC classes derived from object-based and pixel-based classifications. Pixel-based classifications were influenced heavily by the effect of so-called salt and pepper noise (for example see the LULC map produced by classifying the fused image using pixel-oriented RF in fig. 4), whereas in object-based classifications boundaries of LULC polygons were smoother and visually more appealing.

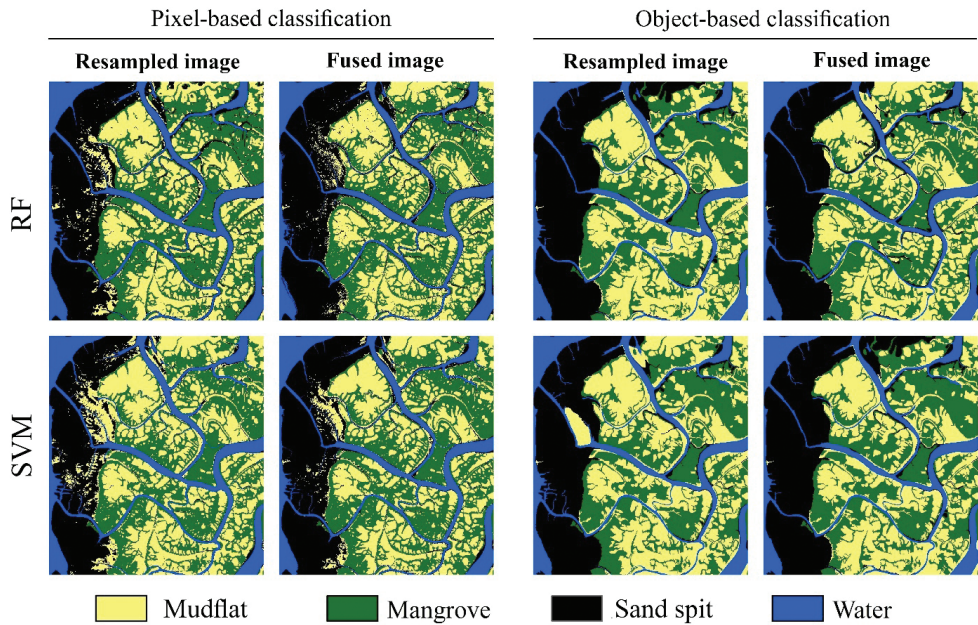


Figure 4. Overview of the subsets of the classification maps derived from object-based and pixel-based classifications, Random Forest (RF) and Support Vector Machine (SVM).

The results of accuracy assessment for each classification are summarized in fig. 5 (due to limited space and for easier comparison of the results, confusion matrices are not shown). In this study, object-based classifications produced more satisfactory results than pixel-based classifications. Kappa coefficient and overall accuracy values obtained from pixel-based classifications were relatively low, below 72.2% and 80.8%, respectively, whereas these values were estimated to be much higher for object-based classifications. None of the object-based classifications represented kappa coefficient and overall accuracy values of less than 85% and 90%, respectively. According to the kappa classification scheme proposed by Monserud and Leemans (1992), pixel-based classifications represented a fair to good level of kappa coefficient (kappa coefficient of between 40% and 75%) while it was categorized as excellent (kappa coefficient of above 75%) for object-based classifications. In terms of the type of imagery data, the fused image was classified more accurately than the resampled image. Furthermore, regardless of the type of imagery data, the accuracy of RF in object-based classifications was higher than the accuracy of SVM while in pixel-based classifications, SVM performed better than RF. Among all classifications, the object-oriented RF classifier applied on the fused Sentinel image outperformed other classifications in terms of kappa coefficient and overall accuracy with values of 93.0% and 95.2%, respectively.

The producer's and user's accuracy statistics were also calculated to find out whether the classifications succeeded in mapping each LULC class. The producer's accuracy, as an indicator depicting how well a class is categorized (the accuracy of classification)

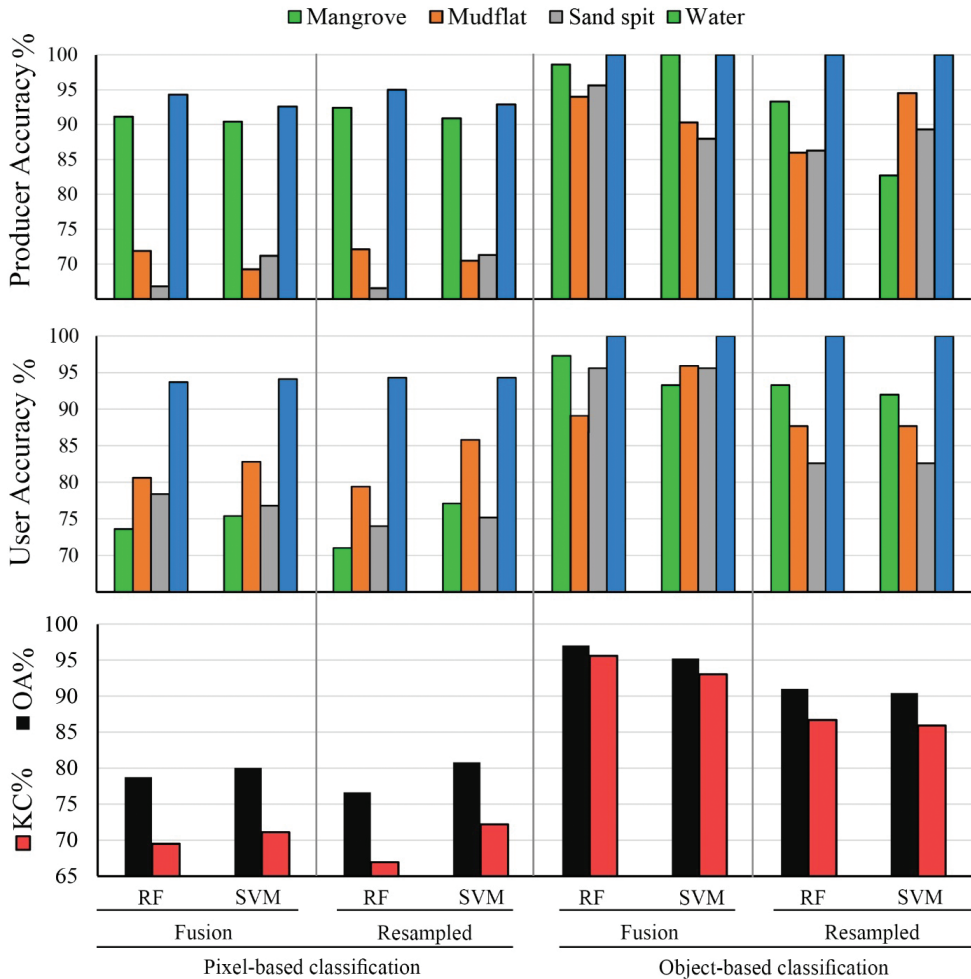


Figure 5. The results of accuracy assessment for each classification, Kappa Coefficient (KC%) and Overall Accuracy (OA%).

(Pelcat 2006), obtained high values for water and mangrove classes under all classifications. Mudflat and sand spit classes were misclassified with each other as well as categorized frequently as mangrove class under pixel-based classifications and yielded relatively low producer's accuracy values, below 73%. From the user's accuracy perspective (as a measure of the reliability of classification (Congalton and Green 2008)), a relatively large proportion of mudflat and sand spit classes pixels were mistakenly labeled as mangrove under pixel-based classifications. In total, object-based classifications achieved higher user's and producer's accuracy values, while in pixel-based classifications, accurate and reliable results were only obtained for water class.

At the patch level, mangrove patches extracted from the pixel-based and object-oriented methods were investigated for both RF and SVM algorithms. The results of

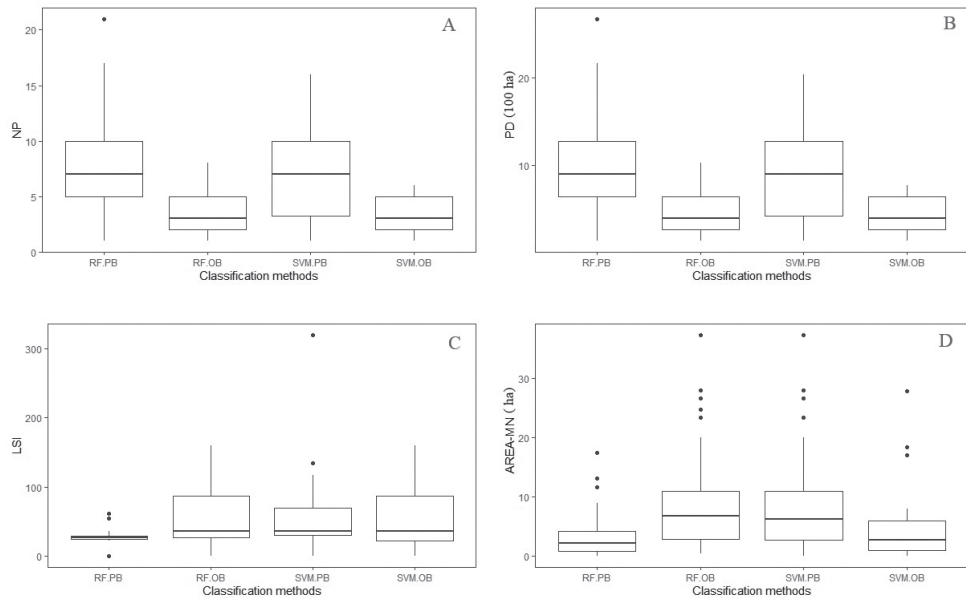


Figure 6. Comparison of **A** number of patch (NP) **B** patch density (PD) **C** landscape shape index (LSI), and **D** Mean Patch Area (AREA-MN) metrics for mangrove patches resulting from fusion image processing using two pixel-based (PB) and object-oriented (OB) methods with two random forest (RF) and support vector machine (SVM) algorithms.

the metrics of NP and PD showed that in the pixel-based method the total number of patches and mangrove patch density was higher than in the object-oriented method and a significant difference was observed between the two algorithms (Fig. 6 (A) and (B)). The results of LSI metric showed that this metric for the pixel-based method is less than the object-oriented method and there is a significant difference between the value of this metric for the pixel-based method between RF and SVM algorithms (Fig. 6 (C)). The AREA-MN metric results showed that the metric value is higher for the pixel-based method with SVM algorithm and the object-oriented method with RF algorithm; however, there was not a significant difference between the classification methods.

At the class and landscape level, metrics were compared for classification maps obtained from the object-oriented method with the RF algorithm and the pixel-based method with the SVM algorithm, which had the highest accuracy (fig. 7). The results of PLAND metric showed that the percentage of mangrove and water class area was similar in both methods, but the mudflat class area was larger for the pixel-based method with SVM algorithm than the object-oriented method with RF algorithm and vice versa for barren class. The results of the NP metric showed that the number of spots for all classes in the pixel-based method with the SVM algorithm was much higher than the object-oriented method. In both methods, the highest number of patches was related to the mudflat class and the lowest was attributed to the water class. The fractal dimension metric was related to the complexity of the patches, which

approaches two if the shape is very complex. The results of fractal dimension metric showed that the value of this metric for the object-oriented method with RF algorithm was less than the pixel-based method with SVM algorithm and the highest value of fractal dimension in both methods was related to the water class. The lowest values for the object-oriented and pixel-based methods were related to the barren and mangrove methods, respectively. The results of ENN-MN metric showed that the amount of this metric for the pixel-based method was less than the object-oriented method. The lowest ENN-MN values in the object-oriented method belonged to the mudflat class and in the pixel-based method to the barren class.

At the landscape level, the results of the metrics are displayed in Table 4. The total number of patches in the object-oriented method with RF algorithm was 1365 and in

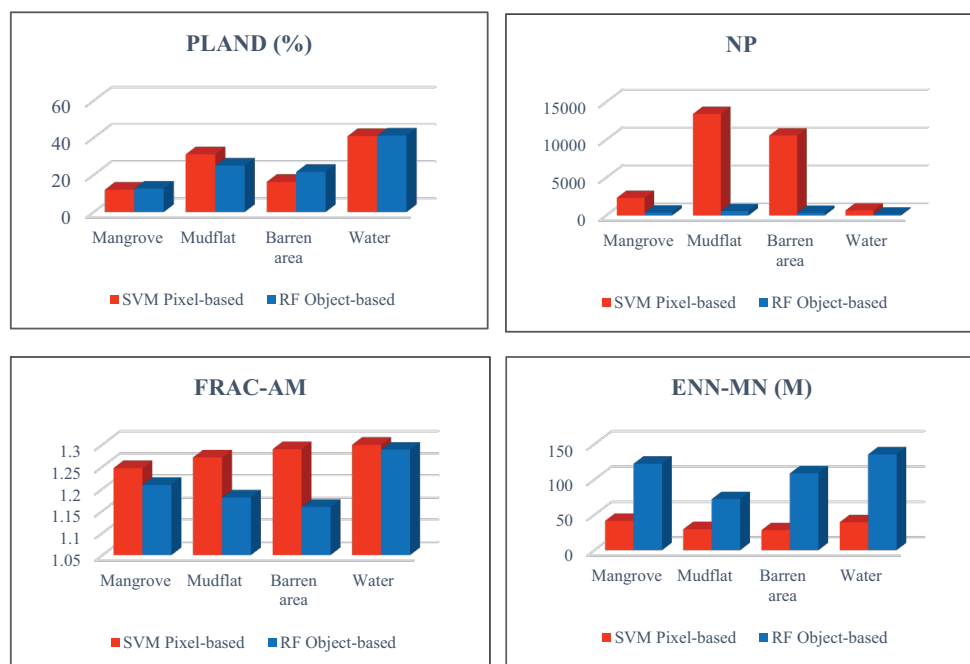


Figure 7. Comparison of landscaping metric results between the classification map obtained from the object-oriented method with random forest (RF) algorithm and the classification map obtained from the pixel-based method with the support vector machine (SVM) algorithm at the class level **A** percentage of landscape (PLAND) **B** number of patch (NP) **C** area Weighted Mean Patch Fractal Dimension (FRAC-AM) **D** Euclidean nearest neighbor distance (ENN-MN).

Table 4. Comparison of landscape metrics for two classification maps using the object-oriented and pixel-based methods at the landscape level.

LID	TA	NP	PD	ED	AREA-MN	FRAC-AM	ENN-MN	CONTAG	SHDI
RF object-based	65659.31	1356	2.06	48.72	48.42	1.20	99.35	48.37	1.30
SVM object-based	65659.32	26982	40.65	101.37	2.44	1.37	30.30	46.11	1.27

the base pixel method with SVM algorithm was 26982. Comparison of the results of metrics at the landscape level also showed that in the pixel-based method with SVM algorithm, the PD and ED increased significantly compared to the object-oriented method with RF algorithm. In the object-oriented method, the AREA-MN metric and the closest distance metric increased. The results of the variability and continuity metrics for the object-oriented method were greater than for the pixel-based method.

Discussion

This study compared the performance of different combinations of satellite images and classification techniques to provide insights for future studies on mangrove LULC classification. In terms of image selection, a growing propensity has emerged recently in using free Sentinel 1/2 images (Liu et al. 2017).

In Sentinel images, fusion can provide an opportunity to take full advantage of both spectral and spatial power of the image bands (Amarsaikhan et al. 2012). Regardless of the type of classification method and algorithm, the fused Sentinel images led to more reliable results. In line with the results of this study, a review by Joshi et al. (2016) showed that 87% of studies which conducted image classification experiments using both resampled and fused images acknowledged the superiority of fused images over the resampled ones in LULC classification. While the results of this study supported the idea that fused Sentinel images may provide better results in mangrove LULC classification, further research still needs to evaluate various image fusion approaches presented for Sentinel images as well as to develop new approaches to make use of all Sentinel's fine resolution (10 m) images. Progress in this research area, alongside conducting further research on comparison of the performance of resampled and fused Sentinel images (especially in mangrove LULC classification), will more effectively help practitioners in utilizing Sentinel images.

Another challenging issue which has increasingly caught the attention of remote sensing experts is the difference between the performance of pixel-based and object-based methods in LULC classification. Studies in this case showed that there is a glaring disparity between the classification results achieved under these methods and that the superiority of them over each other may depend on a number of factors such as the classification extent, spatial pattern and number of LULC classes (Dingle Robertson and King 2011). Moreover, selecting each method depends on the type of LULC data required; for example, if we need to detect objects at the size of image pixels, pixel-based-classification would be a better choice. Regardless of these considerations, the results of this study showed that object-based classification produced more accurate results. In pixel-based classifications, although water areas were accurately identified, sand spit and mudflat pixels were constantly misclassified as mangrove trees and thus obtained low user's and producer's accuracy values. Such a misclassification substantially raised the area estimated for mangrove class. In the same vein, Belgiu and Csillik (2018) found that the accuracy of object-based classifications is relatively higher than pixel-based in classifying Sentinel-2 images.

As given in the introduction section, the majority of studies on LULC classification concluded that non-parametric algorithms can provide better classification results than the parametric ones. Drawing on previous research carried out in this research area, the performances of RF and SVM as two well-known classification algorithms were evaluated in this research. As shown in fig. 5, none of the algorithms scored best under all circumstances. In object-based classifications, RF was found to be the foremost classifier while SVM performed better in pixel-based classifications. Similar to these results, Thanh Noi and Kappas (2017) compared the performance of a set non-parametric algorithms, especially RF and SVM, in classifying Sentinel-2 images and obtained contradictory results under comparable circumstances. Comparison of landscape metrics at the three levels showed that the type of method and algorithm used to prepare thematic maps can affect the results of composite and structural metrics. Area and size dependent metrics are more influenced by the type of classification method. Object-oriented methods reduced NP and PD due to the absence or lower noise in the processing of the images with greater continuity of patches, and as a result, the distance between the patches was greater. Comparison of shape-dependent metrics such as the fractal dimension showed that the pixel-based method reflects the structure of the patches with more complexity. In addition, changes in land cover have a direct impact on the spatial distribution of mangrove forests and often lead to fragmentation at the landscape scale (Toosi et al. 2022). Besides these disturbances, other studies have displayed that land cover change can cause biodiversity losses of animals and plants (Pedrinho et al. 2019). The land cover change can affect ecological functions by modifying their structure and composition. Thus, with the approach applied in this study, the required information on the trend of changes in land cover that affect the successful development and management of mangrove ecosystems can be provided, supporting better planning and decision-making (Toosi et al. 2022).

Conclusion

Mangroves are globally threatened, disappearing and degraded. Monitoring and evaluating changes in the trends of mangrove distributions and dynamics is urgent for the conservation of these ecosystems. The results of this research showed that object-based classification can better distinguish mangrove trees from mudflat and sand spit, while no solid conclusion was drawn in terms of the application of classification algorithms. Moreover, although further investigations are necessary to determine the potential of fused Sentinel images in LULC classification, our results showed that the accuracy of mangrove LULC classification can be well improved by object-oriented classification of fused Sentinel images. Mangrove ecosystems generally consist of the same LULC classes as those categorized in this research. Therefore, further research in our study area or other mangrove ecosystems is needed to strengthen or support the results obtained by this research and, in turn, inform future research on mangrove ecosystems. The findings of this research can contribute to the improvement of management and conservation strategies for these ecosystems being impacted by human activities.

Acknowledgements

This work was supported by the Isfahan University of Technology, Department of Natural Resources.

References

- Amarsaikhan D, Saandar M, Ganzorig M, Blotevogel H, Egshiglen E, Gantuyal R, Nergui B, Enkhjargal D (2012) Comparison of multisource image fusion methods and land cover classification. *International Journal of Remote Sensing* 33(8): 2532–2550. <https://doi.org/10.1080/01431161.2011.616552>
- Angadi AB, Angadi AB, Gull KC (2013) International Journal of Advanced Research in Computer Science and Software Engineering. *International Journal (Toronto, Ont.)* 3(6): 1706–1746.
- As-Syakur AR, Adnyana I, Arthana IN, Nuarsa IW (2012) Enhanced built-up and bareness index (EBBI) for mapping built-up and bare land in an urban area. *Remote Sensing (Basel)* 4(10): 2957–2970. <https://doi.org/10.3390/rs4102957>
- Ballestrín J, Marzo A (2012) Solar radiation attenuation in solar tower plants. *Solar Energy* 86(1): 388–392. <https://doi.org/10.1016/j.solener.2011.10.010>
- Belgiu M, Csillik O (2018) Sentinel-2 cropland mapping using pixel-based and object-based time-weighted dynamic time warping analysis. *Remote Sensing of Environment* 204: 509–523. <https://doi.org/10.1016/j.rse.2017.10.005>
- Belgiu M, Drăguț L (2016) Random forest in remote sensing: A review of applications and future directions. *ISPRS Journal of Photogrammetry and Remote Sensing* 114: 24–31. <https://doi.org/10.1016/j.isprsjprs.2016.01.011>
- Benz UC, Hofmann P, Willhauck G, Lingenfelder I, Heynen M (2004) Multi-resolution, object-oriented fuzzy analysis of remote sensing data for GIS-ready information. *ISPRS Journal of Photogrammetry and Remote Sensing* 58(3–4): 239–258. <https://doi.org/10.1016/j.isprsjprs.2003.10.002>
- Bihamta N, Soffianian AR, Fakheran S, Pourmanafi S (2019) Incorporating CART algorithm and i for mapping Mangrove using Landsat 8 imagery. *Forest Research and Development* 5(4): 557–569.
- Bihamta Toosi N, Fakheran S, Soffianian A (2012) Analysis of landscape pattern changes in Isfahan city during the last two decades. *Proceedings of International Conference on Applied Life Sciences (ICALS2012)*, Turkey, September 2012, ISALS, 149–153.
- Bihamta Toosi N, Soffianian AR, Fakheran S, Pourmanafi S, Ginzler C, Waser LT (2020) Land Cover Classification in Mangrove Ecosystems Based on VHR Satellite Data and Machine Learning—An Upscaling Approach. *Remote Sensing* 12(17): 2684. <https://doi.org/10.3390/rs12172684>
- Blaschke T (2010) Object based image analysis for remote sensing. *ISPRS Journal of Photogrammetry and Remote Sensing* 65(1): 2–16. <https://doi.org/10.1016/j.isprsjprs.2009.06.004>
- Blaschke T, Lang S, Hay G (2008) Object-based image analysis: spatial concepts for knowledge-driven remote sensing applications. Springer Science & Business Media. <https://doi.org/10.1007/978-3-540-77058-9>

- Bozorgi M, Moein M, Nejadkoorki F, Toosi NB (2020) Assessing the effect of water scarcity on crop selection and spatial pattern of croplands in central Iran. *Computers and Electronics in Agriculture* 178: 105743. <https://doi.org/10.1016/j.compag.2020.105743>
- Breiman L (2001) Random forests. *Machine Learning* 45(1): 5–32. <https://doi.org/10.1023/A:1010933404324>
- Brown MI, Pearce T, Leon J, Sidle R, Wilson R (2018) Using remote sensing and traditional ecological knowledge (TEK) to understand mangrove change on the Maroochy River, Queensland, Australia. *Applied Geography (Sevenoaks, England)* 94: 71–83. <https://doi.org/10.1016/j.apgeog.2018.03.006>
- Choi M, Kim H, Cho N, Kim H (2006) An improved intensity-hue-saturation method for IKONOS image fusion. *Pan I*: v2.
- Congalton RG, Green K (2008) Assessing the accuracy of remotely sensed data: principles and practices. CRC Press. <https://doi.org/10.1201/9781420055139>
- Cortes C, Vapnik V (1995) Support-vector networks. *Machine Learning* 20(3): 273–297. <https://doi.org/10.1007/BF00994018>
- Cristianini N, Shawe-Taylor J (2000) An introduction to support vector machines and other kernel-based learning methods. Cambridge University Press. <https://doi.org/10.1017/CBO9780511801389>
- Dingle Robertson L, King DJ (2011) Comparison of pixel-and object-based classification in land cover change mapping. *International Journal of Remote Sensing* 32(6): 1505–1529. <https://doi.org/10.1080/01431160903571791>
- Drăguț L, Csillik O, Eisank C, Tiede D (2014) Automated parameterisation for multi-scale image segmentation on multiple layers. *ISPRS Journal of Photogrammetry and Remote Sensing* 88: 119–127. <https://doi.org/10.1016/j.isprsjprs.2013.11.018>
- Forman RTT, Godron M (1986) *Landscape Ecology*. New York, Wiley, 595 pp.
- Gašparović M, Jogun T (2018) The effect of fusing Sentinel-2 bands on land-cover classification. *International Journal of Remote Sensing* 39(3): 822–841. <https://doi.org/10.1080/01431161.2017.1392640>
- Giri C, Ochieng E, Tieszen LL, Zhu Z, Singh A, Loveland T, Masek J, Duke N (2011) Status and distribution of mangrove forests of the world using earth observation satellite data. *Global Ecology and Biogeography* 20(1): 154–159. <https://doi.org/10.1111/j.1466-8238.2010.00584.x>
- Grêt-Regamey A, Weibel B, Kienast F, Rabe SE, Zulian G (2015) A tiered approach for mapping ecosystem services. *Ecosystem Services* 13: 16–27. <https://doi.org/10.1016/j.ecoser.2014.10.008>
- Ho HC, Knudby A, Xu Y, Hodul M, Aminipouri M (2016) A comparison of urban heat islands mapped using skin temperature, air temperature, and apparent temperature (Humidex), for the greater Vancouver area. *The Science of the Total Environment* 544: 929–938. <https://doi.org/10.1016/j.scitotenv.2015.12.021>
- Hussain M, Chen D, Cheng A, Wei H, Stanley D (2013) Change detection from remotely sensed images: From pixel-based to object-based approaches. *ISPRS Journal of Photogrammetry and Remote Sensing* 80: 91–106. <https://doi.org/10.1016/j.isprsjprs.2013.03.006>
- Jiang D, Zhuang D, Huang Y (2013) Investigation of image fusion for remote sensing application. *New Advances in Image Fusion*. InTech.

- Joshi N, Baumann M, Ehammer A, Fensholt R, Grogan K, Hostert P, Jepsen MR, Kuemmerle T, Meyfroidt P, Mitchard ET, Reiche J, Ryan C, Waske B (2016) A review of the application of optical and radar remote sensing data fusion to land use mapping and monitoring. *Remote Sensing (Basel)* 8(1): 70. <https://doi.org/10.3390/rs8010070>
- Kuenzer C, Bluemel A, Gebhardt S, Quoc TV, Dech S (2011) Remote sensing of mangrove ecosystems: A review. *Remote Sensing (Basel)* 3(5): 878–928. <https://doi.org/10.3390/rs3050878>
- Lee TM, Yeh HC (2009) Applying remote sensing techniques to monitor shifting wetland vegetation: A case study of Danshui River estuary mangrove communities. *Taiwan. Ecological Engineering* 35(4): 487–496. <https://doi.org/10.1016/j.ecoleng.2008.01.007>
- Li C, Wang J, Wang L, Hu L, Gong P (2014) Comparison of classification algorithms and training sample sizes in urban land classification with Landsat thematic mapper imagery. *Remote Sensing (Basel)* 6(2): 964–983. <https://doi.org/10.3390/rs6020964>
- Lillesand T, Kiefer RW, Chipman J (2014) *Remote sensing and image interpretation*. John Wiley & Sons.
- Liu Y, Wang X, Ling F, Xu S, Wang C (2017) Analysis of Coastline Extraction from Landsat-8 OLI Imagery. *Water (Basel)* 9(11): 816. <https://doi.org/10.3390/w9110816>
- Lunetta RS, Lyon JG (2004) *Remote sensing and GIS accuracy assessment*. CRC Press. <https://doi.org/10.1201/9780203497586>
- Mc Garigal K, Marks BJ (1995) FRAGSTATS: spatial pattern analysis program for quantifying landscape structure. USDA Forest Service, Amherst. <https://doi.org/10.2737/PNW-GTR-351>
- McFeeters SK (1996) The use of the Normalized Difference Water Index (NDWI) in the delineation of open water features. *International Journal of Remote Sensing* 17(7): 1425–1432. <https://doi.org/10.1080/01431169608948714>
- Monserud RA, Leemans R (1992) Comparing global vegetation maps with the Kappa statistic. *Ecological Modelling* 62(4): 275–293. [https://doi.org/10.1016/0304-3800\(92\)90003-W](https://doi.org/10.1016/0304-3800(92)90003-W)
- Mountrakis G, Im J, Ogole C (2011) Support vector machines in remote sensing: A review. *ISPRS Journal of Photogrammetry and Remote Sensing* 66(3): 247–259. <https://doi.org/10.1016/j.isprsjprs.2010.11.001>
- Olagoke A, Proisy C, Féret JB, Blanchard E, Fromard F, Mehlig U, de Menezes MM, dos Santos VF, Berger U (2016) Extended biomass allometric equations for large mangrove trees from terrestrial LiDAR data. *Trees (Berlin)* 30(3): 935–947. <https://doi.org/10.1007/s00468-015-1334-9>
- Olmanson LG, Brezonik PL, Finlay JC, Bauer ME (2016) Comparison of Landsat 8 and Landsat 7 for regional measurements of CDOM and water clarity in lakes. *Remote Sensing of Environment* 185: 119–128. <https://doi.org/10.1016/j.rse.2016.01.007>
- Pedrinho A, Mendes LW, Merloti LF, Da Fonseca MDC, Cannavan FDS, Tsai SM (2019) Forest-to-pasture conversion and recovery based on assessment of microbial communities in Eastern Amazon rainforest. *FEMS Microbiology Ecology* 95(3): fiy236. <https://doi.org/10.1093/femsec/fiy236>
- Pelcat YS (2006) Soil landscape characterization of crop stubble covered fields using Ikonos high resolution panchromatic images. <http://hdl.handle.net/1993/224>

- Pham TD, Xia J, Ha NT, Bui DT, Le NN, Tekeuchi W (2019a) A review of remote sensing approaches for monitoring blue carbon ecosystems: Mangroves, seagrasses and salt marshes during 2010–2018. *Sensors (Basel)* 19(8): 1933. <https://doi.org/10.3390/s19081933>
- Pham TD, Yokoya N, Bui DT, Yoshino K, Friess DA (2019b) Remote sensing approaches for monitoring mangrove species, structure, and biomass: Opportunities and challenges. *Remote Sensing (Basel)* 11(3): 230. <https://doi.org/10.3390/rs11030230>
- Poursanidis D, Chrysoulakis N, Mitraka Z (2015) Landsat 8 vs. Landsat 5: A comparison based on urban and peri-urban land cover mapping. *International Journal of Applied Earth Observation and Geoinformation* 35: 259–269. <https://doi.org/10.1016/j.jag.2014.09.010>
- Proisy C, Viennois G, Sidik F, Andayani A, Enright JA, Guitet S, Gusmawati N, Lemonnier H, Muthusankar G, Olagoke A, Prospero J, Rahmania R, Ricout A, Soulard B, Suhard J (2018) Monitoring mangrove forests after aquaculture abandonment using time series of very high spatial resolution satellite images: A case study from the Perancak estuary, Bali, Indonesia. *Marine Pollution Bulletin* 131: 61–71. <https://doi.org/10.1016/j.marpolbul.2017.05.056>
- Qadri S, Khan DM, Qadri SF, Razzaq A, Ahmad N, Jamil M, Nawaz Shah A, Shah Muhammad S, Saleem K, Awan SA (2017) Multisource data fusion framework for land use/land cover classification using machine vision. *Journal of Sensors* 2017: 1–8. <https://doi.org/10.1155/2017/3515418>
- Ranaie M, Soffianian A, Pourmanafi S, Mirghaffari N, Tarkesh M (2018) Evaluating the statistical performance of less applied algorithms in classification of worldview-3 imagery data in an urbanized landscape. *Advances in Space Research* 6(61): 1558–1572. <https://doi.org/10.1016/j.asr.2018.01.004>
- Salem ME, Mercer DE (2012) The economic value of mangroves: A meta-analysis. *Sustainability (Basel)* 4(3): 359–383. <https://doi.org/10.3390/su4030359>
- Sanli FB, Abdikan S, Esetlili MT, Sunar F (2017) Evaluation of image fusion methods using PALSAR, RADARSAT-1 and SPOT images for land use/land cover classification. *Photonirvachak (Dehra Dun)* 45(4): 591–601. <https://doi.org/10.1007/s12524-016-0625-y>
- Savari M, Damaneh HE, Damaneh HE (2022) Factors involved in the degradation of mangrove forests in Iran: A mixed study for the management of this ecosystem. *Journal for Nature Conservation* 66: 126153. <https://doi.org/10.1016/j.jnc.2022.126153>
- Sothe C, Almeida C, Liesenberg V, Schimalski M (2017) Evaluating Sentinel-2 and Landsat-8 Data to Map Successional Forest Stages in a Subtropical Forest in Southern Brazil. *Remote Sensing (Basel)* 9(8): 838. <https://doi.org/10.3390/rs9080838>
- Srivastava M, Arora MK, Raman B (2015) Selection of critical segmentation—a prerequisite for object based image classification. *Recent Advances in Electronics & Computer Engineering (RAECE), 2015 National Conference on IEEE*. <https://doi.org/10.1109/RAECE.2015.7510243>
- Thanh Noi P, Kappas M (2017) Comparison of Random Forest, k-Nearest Neighbor, and Support Vector Machine Classifiers for Land Cover Classification Using Sentinel-2 Imagery. *Sensors (Basel)* 18(1): 18. <https://doi.org/10.3390/s18010018>
- Tong Yang X, Liu H, Gao X (2015) Land cover changed object detection in remote sensing data with medium spatial resolution. *International Journal of Applied Earth Observation and Geoinformation* 38: 129–137. <https://doi.org/10.1016/j.jag.2014.12.015>

- Toosi NB, Soffianian AR, Fakheran S, Pourmanafi S, Ginzler C, Waser LT (2019) Comparing different classification algorithms for monitoring mangrove cover changes in southern Iran. *Global Ecology and Conservation* 19: e00662. <https://doi.org/10.1016/j.gecco.2019.e00662>
- Toosi NB, Soffianian AR, Fakheran S, Waser LT (2022) Mapping disturbance in mangrove ecosystems: Incorporating landscape metrics and PCA-based spatial analysis. *Ecological Indicators* 136: 108718. <https://doi.org/10.1016/j.ecolind.2022.108718>
- Tran LX, Fischer A (2017) Spatiotemporal changes and fragmentation of mangroves and its effects on fish diversity in Ca Mau Province (Vietnam). *Journal of Coastal Conservation* 21(3): 355–368. <https://doi.org/10.1007/s11852-017-0513-9>
- Uuema E, Mander Ü, Marja R (2013) Trends in the use of landscape spatial metrics as landscape indicators: A review. *Ecological Indicators* 28: 100–106. <https://doi.org/10.1016/j.ecolind.2012.07.018>
- Vo QT, Oppelt N, Leinenkugel P, Kuenzer C (2013) Remote sensing in mapping mangrove ecosystems—An object-based approach. *Remote Sensing (Basel)* 5(1): 183–201. <https://doi.org/10.3390/rs5010183>
- Wang L (2005) Support vector machines: theory and applications. Springer Science & Business Media. <https://doi.org/10.1007/b95439>
- Wang L, Sousa W, Gong P (2004) Integration of object-based and pixel-based classification for mapping mangroves with IKONOS imagery. *International Journal of Remote Sensing* 25(24): 5655–5668. <https://doi.org/10.1080/014311602331291215>
- Wang Q, Shi W, Li Z, Atkinson PM (2016) Fusion of Sentinel-2 images. *Remote Sensing of Environment* 187: 241–252. <https://doi.org/10.1016/j.rse.2016.10.030>
- Wulder MA, Masek JG, Cohen WB, Loveland TR, Woodcock CE (2012) Opening the archive: How free data has enabled the science and monitoring promise of Landsat. *Remote Sensing of Environment* 122: 2–10. <https://doi.org/10.1016/j.rse.2012.01.010>
- Xu H (2006) Modification of normalised difference water index (NDWI) to enhance open water features in remotely sensed imagery. *International Journal of Remote Sensing* 27(14): 3025–3033. <https://doi.org/10.1080/01431160600589179>
- Zahed MA, Rouhani F, Mohajeri S, Bateni F, Mohajeri L (2010) An overview of Iranian mangrove ecosystems, northern part of the Persian Gulf and Oman Sea. *Acta Ecologica Sinica* 30(4): 240–244. <https://doi.org/10.1016/j.chnaes.2010.03.013>
- Zarezadeh R, Rezaee P, Lak R, Masoodi M, Ghorbani M (2017) Distribution and accumulation of heavy metals in sediments of the northern part of mangrove in Hara Biosphere Reserve, Qeshm Island (Persian Gulf). *Soil and Water Research* 12(2): 86–95. <https://doi.org/10.17221/16/2016-SWR>
- Zhang H, Wang T, Liu M, Jia M, Lin H, Chu L, Devlin A (2018) Potential of Combining Optical and Dual Polarimetric SAR Data for Improving Mangrove Species Discrimination Using Rotation Forest. *Remote Sensing (Basel)* 10(3): 467. <https://doi.org/10.3390/rs10030467>